RSC Advances

This is an *Accepted Manuscript*, which has been through the Royal Society of Chemistry peer review process and has been accepted for publication.

Accepted Manuscripts are published online shortly after acceptance, before technical editing, formatting and proof reading. Using this free service, authors can make their results available to the community, in citable form, before we publish the edited article. This *Accepted Manuscript* will be replaced by the edited, formatted and paginated article as soon as this is available.

You can find more information about *Accepted Manuscripts* in the Information for Authors.

Please note that technical editing may introduce minor changes to the text and/or graphics, which may alter content. The journal's standard Terms & Conditions and the Ethical guidelines still apply. In no event shall the Royal Society of Chemistry be held responsible for any errors or omissions in this *Accepted Manuscript* or any consequences arising from the use of any information it contains.

ROYAL SOCIETY OF CHEMISTRY

www.rsc.org/advances

PEG-assisted hydrothermal synthesis and electrochemical performance of ZnO/Ketjenblacknanocomposite for lithium ion batteries

Chao Chen[a], *Huang Zhang* [b], *Yunlong Xu*[*a], *Mandi Ji*[a], *Hui Dong*[a],*Chongjun, Zhao*[a]

Abstract

ZnO/Ketjenblack(KB)composite was fabricated by means of a facile PEG-assisted hydrothermal synthesis process, characterized by X-ray powder diffraction, scanning electron microscopy, field emission transmission electron microscopy,thermogravimetricanalysis, nitrogen sorption,Energy Dispersion Spectroscopy, galvanostastic charge/discharge test, Cyclic Voltammogram and Electrochemical impedance spectroscopies. The results show that the composite forms a special porous structurewith ZnO particles embedded in the mesopores of Ketjenblack, which favors the improvement of electrochemical performance. Compared with unmodified ZnO, ZnO/KB composite exhibits superior electrochemical performances. ZnO/KB composite delivers a discharge capacity of 418.9 $mAh \cdot g^{-1}$ at the discharge density current of 800 $mA \cdot g^{-1}$, whereas the ZnO only gives 116.1 $mAh \cdot g^{-1}$. Moreover, the sample retains a discharge capacity of 538.4 $mAh \cdot g^{-1}$ after 100 cycles at a current density of 100 $mA \cdot g^{-1}$. The improved electrochemical performance can be ascribed to the combined Ketjenblack, which serves as conducting buffering matrix during lithiation/delithiation process.

Introduction

RSC Advances Accepted Manuscript

Recently, due to the high theoretical capacity of 978 mAh/g[1], which is twice times larger than that of graphite anode (~370 mAh·g^{-1})[2, 3], ZnO is attracting more and more attentions as alternative anode material to graphite in LIBs. However, severe capacity fading, caused by the intrinsic low conductivity and the pulverization arising from the large volume change during lithiation/delithiation process, hinders its practical application[4, 5]. Hitherto, a lot of efforts have been devoted to overcoming these problems and many approaches have been adopted.It has been reportedthattheelectrochemical propertiesofZnOcanbeimprovedby(i)doping and forming composite with metal, metal oxide or carbonaceous materials[6-8]; (ii)creatingvoid space in the structure[9]; (iii)preparingorderedstructured materials[10, 11];(iv)downsizing the particle[12].

Inspired by the above results, downsizing the particleoccurs to an efficient way to improve their electrochemical properties. Many approaches have been employed to synthesize ZnO nanostructures, includingchemical vapor deposition[13], physical vapordeposition[14], electrodeposition[15]and hydrothermal process. Among all kinds of adopted methods, the hydrothermal processseems to be a promising aqueous-based precipitation route, allowing control over the nucleation and crystal growth by simply tuning the hydrothermal reaction conditions. Poly ethylene glycol (PEG), as a conventional polymer surfactant to control the orientation and dimension of ZnO, hasbeen used to construct diverse morphologies of ZnO during the hydrothermalsynthesis process[16, 17].

Meanwhile, Ketjenblack is a highly conductive carbon with a typically

RSC Advances Accepted Manuscript

mesoporous structure[18]. Using theKetjenblack to achieve a novel nano/mesoporous structure has alreadybeen reported[19-21]. Owing to the mesoporousstructureand conductivecharacter,Ketjenblackcan not only strengthen the electron conduction, but also effectively prevent the pulverization and agglomerationfrom the volume change during the charge/discharge process, which consequently leads to aremarkable improvement in cyclingcapability.

Herein, we reported a facile PEG-assisted hydrothermal method to synthesize the ZnO/KB nanocomposite with an open 3D network structure and the electrochemical performances as the anode material for lithium-ion batteries were investigated.

Experimental section

Sample preparation

All chemicals are ofanalytical reagent grade and used without further purification.ZnO/KB composites were synthesized by precipitationfrom aqueous solution under hydrothermal condition in the following way:

The first step: $Zn(NO_3)_2 \cdot 6H_2O$, $(NH_4)_2CO_3$ and polyethylene glycol(PEG, molecular weight:2,000) were dissolved in distilled water to form 1.0 M $Zn(NO_3)_2$ solution, 1.0M $(NH_4)_2CO_3$ solution and 0.4% PEG solution, respectively. Then stoichiometric amounts of zinc nitrate hexahydrate and KetjenblackEC 300J(akzonobel) were mixed in 150 mL distilled water with fully constant stirring, then repeatedly filtrated to obtain the precursors. After that, the precursors wereimmersed with the filtrate to form suspension. With vigorous constant

RSC Advances Accepted Manuscript

stirring,20mL of 1.0 M $(NH_4)_2CO_3$ solutionwere added dropwise intothe above suspension at 25°C. Precipitateswere collected, and washed with deionized water and ethanolseveral times,respectively.

The second step: After washed, the resulting precipitateswere dispersedin 0.4% PEG (2000) solution and transferred into aTeflon-lined autoclave. After being sealed, theautoclave was put into an oven and maintained at200 °C for 10 h. After cooling down to room temperature, the deposited ZnO/KB composite were washed with deionized water and alloweddrying at 80 °C.As reference, the bulk ZnO particles were hydrothermally synthesized under the same conditionsby removing KB.

Sample characterization

X-ray powder diffraction (XRD) patterns were collected by X-ray diffractometer(D/MAX 2550V, Japan) with Cu K_a (k =1.5406 Å). The morphology and particle structure of as-preparedZnO sample were characterized by scanning electron microscopy(SEM, S-3400N) and field emission transmission electron microscopy (TEM,JEM-2100, Japan). The thermogravimetric analysis (TGA) was carried out on a SDT-Q600 thermal analyzerto evaluate the carbon content. The Brunauer-Emmett-Teller (BET) surfacearea and pore size distribution were evaluated on a TriStar 3000system.

Electrochemical measurements

CR2032 coin cells were fabricated in an argon-filled glove box (MIKROUNA)for electrochemical measurements. The synthesized samples were mixed with acetylene blackand polyvinylidene fluoride (PVDF)in the weight ratio of

RSC Advances Accepted Manuscript

8:1:1 by blendingin N-methyl-2-pyrrolidone (NMP). The resultant slurries were then pasted on copper foil and driedat 120 °C for 12 h under vacuum environment. After drying, the samples were used as anode. Lithium foil was used as both counter electrodes and the electrolyte was 1M $LiPF_6$ in ethylene carbonate (EC)/diethyl carbonate (DEC) (1:1 in volume). A Celgard 2400 mesoporous membrane was used as the separator. The cells were aged for 12h before measurement. The charge/discharge test was carried out with a LAND Battery Program-control Test System (CT2001A,China) over a voltage range of 0.01~3.0V.Cyclic Voltammogram (CV: 0.1mV s^{-1},0.01~3V) tests were conducted on an Electrochemical Workstation (CHI, 660B, CHENHUA, China). Electrochemical impedance spectroscopies(EIS) of the cells were also conducted on the Electrochemical Workstation. The EIS spectra were potentiostatically collected by using a DC potential equal to the open circuit voltage of the cell and an AC oscillation of 5mV over a frequency range of 10^5Hz–0.01Hz. All tests were performed at room temperature(25°C).

Results and discussion

Fig. 1is the schematic diagram of ZnO/KB composite formation. In the process of ZnO formation, $ZnCO_3$ wasformedin the pore of KB with the filtration process as theprecursor[22].With the presence of a water-soluble polymer(PEG 2000), which actedas both the catalyst andsurfactant[23], zinc oxide crystals form heterogeneous nucleus in the pore and the interface of KB by the dehydration of $ZnCO_3$. Finally, the formation of ZnO/KB composite completes totally after hydrothermal treatment. The

RSC Advances Accepted Manuscript

nonionic surfactant PEG with a uniform and ordered chain structure has a great influence on the growth process of ZnO[16, 17]. The small ZnO crystal grains will be enwrapped into the coil of PEG and form agglomerates. According to the theory of crystal growth thermodynamics in the oversaturated solution[16], numerous small ZnO grains will be dissolved or recrystallized at a thermodynamic balance state. Only the large crystalline grains, whose size is larger than the critical size, would grow up spontaneously, while the smaller ones under the critical size will redissolve into solution. On this level, the PEG coils here just provide assistance to the crystallization of ZnO crystals and the coalescence of adjacent crystalline grains[16]. Thus, the PEG provides the active sites for ZnO crystalline growth. As we discussed above, it is well known that the interaction between PEG and zinc species could accelerate the nucleation, and the coiled agglomerate could be in favor of the crystallization of ZnO crystal grains.

Shown in Fig. 2 are the XRD patterns of ZnO/KB nanocomposite, ZnO and KB, as well as the JCPDS standard diffraction patterns of ZnO, respectively. All the diffraction peaks of ZnO/KB can be indexed as the featured hexagonal phase of ZnO with the lattice constants a=3.246Å, b=3.231 Å, c=5.2092 Å, which is in good agreement with the standard data of JCPDS CARD No.36-1451(a=3.250Å, b=3.250 Å, c=5.2071 Å). These results imply the prepared ZnO was well crystallized. This consistency illuminates that the emergence of KB have no effect to the hydrothermal synthesis. Apart from ZnO diffraction peaks, no additional peaks can be detected, mirroring the high purity of the product. Additionally, the slight protuberance between

RSC Advances Accepted Manuscript

15°and 30° in the XRD pattern of ZnO/KB can be ascribed to the amorphous KB, which is consistent with the broad peak of KB in the range of 15~30° shown in XRD results.

The carbon content of ZnO/KB was measured by the thermogravimetric (TG) technique under an ambient atmosphere. As shown in Fig. 3, the two weight loss peaks at 71 °C and 320 °C correspond to the removal of physically adsorbed water and the thermal decomposition of KB,respectively.The mass remains unchanged after 500 °C. The weight loss between 320 and 500 °C can be ascribed to the oxidization and subsequent decomposition of KB, and the value can be considered as the carbon content. Hence, the carbon content of the as-obtained ZnO/KB is calculated to be 24.94%.

The nitrogen adsorption-desorption isotherm and pore size distribution curves (inset) of KB and ZnO/KB composite are shown in Fig. 4. According to the IUPAC classification[24], the isotherm shows a typical V isotherm with H1 hysteresis loop for both the KB and the ZnO/KB nanocomposite, indicating the mesoporous structure. The BET surface area, pore volume and pore diameter of the samples are listed in Table 1. As shown in Table 1, the values of the above parameters are 549.54m^2g^{-1}, 0.69cm^2g^{-1}, 3.63nm for the ZnO/KB composite and 1265.92 m^2g^{-1}, 3.01 cm^2g^{-1}, 7.199 nmfor KB, respectively. The large surface area of KB was benefit to absorption of PEG, which promoted the nucleation of ZnO. Compared to the KB, the decreased values of ZnO/KB composite can be attributed to the embedding of ZnO nanoparticles in mesopores of KB. The large surface area provides more electrochemical active sites

RSC Advances Accepted Manuscript

and the porosity can also broaden an effective channel for the diffusion of Li^+ and electrons, which is beneficial to improve the electrochemical properties of electrode materials[25].

The SEM images of pure ZnO, pristine KB and ZnO/KB are as shown in Fig. 5. Fig. 5(a) andFig. 5(b) show the morphology of pure ZnO, which is in accordance with the above discussion of the formation of ZnO crystals.ZnO crystals grow up along the chains of PEG to form nanorods[22] as showed in Fig. 5(b). Fig. 5(c) and Fig. 5(d) show the structure of pristine KB and ZnO/KB composite, respectively. Compared to porous morphology of pristine KB, the similarly loosely-restacked and porous structures are observed in ZnO/KB composite. This result combined with BET results indicate that the load of ZnO will not change the overall skeletons and porous structure of KB, and ZnO is embedded into the KB skeletons without apparent clusterwhich brings the pore size change of KB.The mesoporous structure of ZnO/KB will be beneficial to accommodate the volume variations and facilitate the electron transfer/Li^+ diffusion.

To further confirm the existence of ZnO in the KB, TEM measurement was carried out. The TEM images of ZnO/KB composite are shown in Fig. 6.Fig. 6(b) is the magnification picture of the red circled area in Fig. 6(a). The red circled area was marked to note the area where the lattice fringes appeared. The highly ordered crystalline of ZnO nanoparticles are clearly seen in the red circle in Fig. 6(b), which confirms the existence of ZnO in the pores of KB. Also Fig. 6(b) clearly reveals that ZnO nanoparticles with a diameter of 10nm are decorated in the mesoporous networks

RSC Advances Accepted Manuscript

of KBfrom the lattice fringes. Such structure can efficiently increase the contact area between electrolytes and active ZnO particles, thereby boosting the transportation of lithium-ions.

In order to investigate the uniform dispersion of ZnO nanoparticles in KB,the elemental mapping of ZnO/KB sample was analyzedby Energy Dispersion Spectroscopy (EDS)measurement. Fig. 7(a) shows the SEM image of the tested area,the integral and separate distributionof the ZnO, O and C elements in the tested area is presented in Fig. 7(b). Fig. 7(c,d,e)exhibit the separate distributions of the different elements O, C and Zn in the area, respectively. As presented in Fig. 6(c,e), the elements ZnO and O have homogeneous distributions, which are rendered as evidence of successful disperse of ZnO in the mesopores of KB through hydrothermal reactions.

Fig. 8(a) displays the cyclic voltammograms (CVs) of ZnO/KB composite and ZnO at a scan rate of 0.1 mV s^{-1}in the voltage ranging from 0.01 to 3 V.For the electrode of ZnO/KB, in the first cycle, two cathodic peaks are observed at about 0.50 and 0.25 V. The strong reduction peak at 0.25 V is due to the generation of Li-Zn alloy together with the decomposition of electrolyte and the resulting growth of organic-like solid electrolyte interphase (SEI) layer, while the relative weak peak at about 0.5 V is related to a combination of several electrochemical reactions with close potentials, such as the reduction of ZnO into metallic Zn and the formation of amorphous Li_2O[10, 26, 27]. During the subsequent anodic scan, there are five different oxidation peaks, located at 0.37, 0.54, 0.69, 1.38 and 2.6V. The first four can be

RSC Advances Accepted Manuscript

ascribed to a multi-step dealloyingprocess of lithium-zinc alloy (LiZn, Li_2Zn_3, $LiZn_2$ and Li_2Zn_5) and the decomposition of the organic-like-layer[8, 26, 28, 29]. The last peak is found at 2.6V and it corresponds to the formation of ZnO[30].In the second cycle, the cathodic peak shifts significantly from 0.5 V to a higher potential of 0.74 V while the anodic peak happens lightly. From the second cycle onwards, the CV curves almost superpose in shapes, implying high reversibility of the electrochemical reactions. The CV results of ZnO are smaller than that of ZnO/KB. And the corresponding peaks in ZnO curves are not conspicuous in the CV cycle, due to their smaller specific surface areas and the longer diffusion distances.

According to above results and previous studies, the Li-storage mechanism of ZnO/KB owns to two reversible electrochemical reactions as below[27, 31]:

(1)

(2)

Fig. 8(b) discloses the initial two charge-discharge curves of ZnO and ZnO/KB-based electrodes at 100 mA g^{-1}in the voltage range of 0.01~3.0 V(vs. Li^+/Li). Two plateaus in the initial discharge curve can be observed. The long flat plateau near 0.5 V corresponds to the reduction of ZnO into Zn as well as the formation of Li_2O, while the slight plateau appeared around 0.25 V may be assigned to the decomposition of electrolyte and formation of lithium-zinc alloy, which is coincide with the above CV results[1, 12, 28].

In the second discharge curve, the long plateau is replaced by a slope between 1.1 and 0.3 V, which is similar with other ZnO-based electrodes reported previously[11,

RSC Advances Accepted Manuscript

[27, 32]. However, no obvious plateaus can be observed in the charge curves.

The initial discharge capacities of ZnO/KB and ZnO are 1346.1 and 997.7 $mAh \cdot g^{-1}$, respectively, much higher than the theoretical value of 978 $mAh \cdot g^{-1}$. The excess capacity might originate from electrolyte decomposition in the low-potential region, formation of solid electrolyte interface (SEI) layer and perhaps abundant specific surface area as well as the good dispersity of the ZnO in KB, which would enhance the surface electrochemical reactivity and improve Li-ion storage capacity[33, 34]. The second discharge capacities of ZnO/KB and ZnO are 718.7 and 585.2 $mAh \cdot g^{-1}$since irreversible SEI formation is nearly completed after the first lithium insertion and extraction process[29, 35].

Fig. 8(c) shows the long-term cycling performances and the corresponding Coulombic efficiencies of the ZnO/KB, ZnO and KB at100mA/gbetween 0.01and 3V. The top two curves are the coulombic efficiencies of the ZnO/KB and ZnO, respectively.The initial discharge capacity of ZnO/KB, ZnO and KB are 1206.8, 798.7 and 360.9 $mAh \cdot g^{-1}$. During the first 10th cycles, a large capacity fading can be found in ZnO/KB, while the capacity maintains at about 550$mAh \cdot g^{-1}$ up to 100 cycles with no further significant fading. After 100 cycles, ZnO/KB, ZnO and KB exhibit a reversibility capacity of 538.4, 185.05 and 216.5 $mAh \cdot g^{-1}$. Furthermore, in order to demonstrate the function of the structure of KB, the capacities of ZnO from ZnO/KB were calculated by eliminating the proportion of capacity from KB, as showed in Fig. 8(c). The capacity contributed by ZnO in ZnO/KB can be calculated as 484.5 $mAh \cdot g^{-1}$after 100 cycles.Thus the ZnO in the composite shows a relative high

RSC Advances Accepted Manuscript

reversible capacity and excellent cycling stability in comparison with bulk ZnO. Normally, the repeated volume change during the lithium ions insertion/extraction process results in the particle pulverization and electrode deterioration. Hence, the excellent superior cycle performance of the composite can be overwhelmingly attributed to its porosity created by KB skeletons and mirrored the integrity of the ZnO/KB electrode.

The rate capabilities of all samples were also measured from 100 $mA \cdot g^{-1}$ to 800 $mA \cdot g^{-1}$ and the results are depicted in Fig. 8(d). Compared to pristine ZnO, ZnO/KB displays a superior rate capability. The average reversible capacities of ZnO/KB drop from 701, 587.4, 505.3 to 418.9 $mAh \cdot g^{-1}$ as the current densities increase from 100, 200, 500 to 800 $mA \cdot g^{-1}$. Moreover, after being cycled at high rates, the capacity of ZnO/KB can well recover to 627.8 $mAh \cdot g^{-1}$once the current density is shifted to the original low value, indicating the excellent reversibility of ZnO/KB electrode.

To further understand the role of KB combination on the electrochemical performance of ZnO anode material, electrochemical impedance spectroscopy (EIS) measurements were performed in a frequency range from 0.01 to 10^5 HZ and the Nyquist plots are given in Fig. 9(a).It can be seen clearly that the impedance spectrum of ZnO and ZnO/KB were composed of a sloping line in the low frequency range and a depressed semicircle in high frequency. The high frequency intercept at the real axis corresponds to bulk resistance (R_e) of the cell, which reflects the electronic conductivity of the electrolyte, separator and electrode. The sloping line in the low frequency region is related to Warburg impedance (W), which is associated withthe

RSC Advances Accepted Manuscript

Li-ions diffusion in thebulk electrode. The Nyquist plots are fitted using an equivalent circuit asshown in the insert of Fig. 9(a), and the derived impedance parameters of R_e, R_{ct}(the charger-transfer reaction resistance),W are listed in the Table 2 .The R_{ct} value of ZnO/KB is much smaller than that of ZnO, which means the lower charger-transfer resistance of the ZnO/KB.

The diffusion coefficient values of the lithium ions (D_{Li+}) in thebulk electrodecan be calculated from the followingEq. 1 [37].

$$D_{Li^+} = \frac{R^2T^2}{2A^2n^4F^4C^2\sigma_w{}^2} \quad (1)$$

where R is the gas constant (8.314Jmol^{-1}K^{-1}), T is the absolute temperature in Kelvin(298.15K), A is the area of the electrode surface, n is the number of electrons per molecule during oxidization, F is theFaraday's constant (96,500Cmol^{-1}), C is the concentration of lithium ion in solidand σ_w is the Warburg coefficient, ρ is density of thesynthesized materials, M is molecular weight of ZnO.The σ_w can be calculated by the following Eq. 2[37].

$$Z_{re} = R_e + R_{ct} + \sigma_w \omega^{-1/2} \quad (2)$$

where Z_{re} is the real part of the impedance, R_e is the resistance ofthe electrolyte, R_{ct} is the charge transfer resistance and ω is theangular frequency in the low frequency region. Both R_e and R_{ct} arekinetics parameters independent of frequency. And$\sigma_w$is the slopefor the plot of Z_{re} vs. the reciprocal root square of the lower angularfrequency ($\omega^{-1/2}$).The plot of Z_{re} vs. the reciprocal root square of the lower angularfrequencies ($\omega^{-1/2}$) for the two samples is shown in Fig. 9 (b)**.**The σ_w values of ZnO/KB and ZnO are 19.53Ωcm$^2\cdot$ s$^{1/2}$ and 92.48Ωcm$^2\cdot$s$^{1/2}$, as shown in Table 2.

RSC Advances Accepted Manuscript

According to the Eq. 2, the D_{Li}^{+} value is in inverseproportion to the σ_w value. As a consequence, the value of D_{Li}^{+} for ZnO/KB is higher than that of ZnO. The decreased charger-transfer resistance and enhanced diffusion coefficient can be mainly attributed to the combination of conducive KB, which can maintain the structure of ZnO, construct a network to shorten the lithium ion diffusion length hinders particle agglomeration and enlarge the electrode/electrolyte contact surface.

Overall, the enhanced electrochemical performance of ZnO/KB composite can be attributed to its mesoporous structure and extra carbon support. Specifically, KB has a large specific surface area of $822.7 m^2 \cdot g^{-1}$[18], which can provide large contact interfaces between electrode and electrolyte. Moreover, the porosity of KB canalso efficiently shorten the Li ion insertion/extraction distance and accommodate the volume change to alleviate the pulverization, resulting in the higher capacity and enhanced rate capability[25, 36]. Thus, the KB, as a kind of carbonous material, can not only improve the conductivity of electrodes, but also provide extra support to the structures, which plays a positive role in the high reversible capacity and excellent cyclability of the fabricated electrodes[38].These aspects give a result of the improvements of the electrochemical properties of the ZnO/KB composite material.

Conclusions

In summary, ZnO/KB nanocomposite wassynthesized through a facilePEG-assistedhydrothermal route. The prepared nanocomposite exhibits a relative high specific capacity, excellentcyclability and high rate capability compared

RSC Advances Accepted Manuscript

with the pure ZnO. The as-improved performances of ZnO/KBcan be attributed to the intrinsic features of KB, namely the mesoporous structure and conductively, which can kinetically advance the ion diffusionin the active materials, efficientlyaccommodate the huge volume expansion during the discharge /charge processesand significantly enhance the conductivity of active materials.Therefore, the ZnO/KB nanocomposite anode for LIBs achieves significant improvementin reversible capacity and cycle stability over the pure ZnO.This novel and facile method may be extended to prepare other materialsfor lithium ion batteries.

Acknowledgments

The work is supported by Shanghai Nanotechnology SpecialFoundation (No. 11nm0500900), Shanghai Leading Academic Discipline Project (No. B502) and Shanghai Key Laboratory Project (No.08DZ2230500).

Notes and Reference

[a] *Key Laboratory for Ultrafine Materials of Ministry of Education, Shanghai Key Laboratory of Advanced Polymeric Materials, School of Materials Science and Engineering, East China University of Science and Technology, Shanghai 200237, PR China*

Fax: +86-021-64250838; Tel.: +86-021-64252019;

E-mail:wuanjun007@163.com (C.C);xuyunlong@ecust.edu.cn(Y.L. Xu)

[b]*Department of Materials Engineering (MTM), KU Leuven, KasteelparkArenberg 44, B-3001 Leuven, Belgium*

1. Q. Pan, L. Qin, J. Liu, H. Wang, Electrochimica Acta, 2010, 55, 5780-5785.
2. H. B. Wu, J. S. Chen, H. H. Hng, X. W. Lou, Nanoscale, 2012, 4, 2526-2542.
3. H. Buqa, D. Goers, M. Holzapfel, M. E. Spahr, P. Novák, Journal of the

RSC Advances Accepted Manuscript

Electrochemical Society, 2005, 152, A474-A481.

4. F. Belliard, P. Connor, J. Irvine, Solid State Ionics, 2000, 135, 163-167.
5. H. Li, Z. X. Wang, L. Q. Chen, X. J. Huang, Advanced Materials, 2009, 21, 4593-4607.
6. W. T. Song, J. Xie, S. Y. Liu, Y. X. Zheng, G. S. Cao, T. J. Zhu, X. B. Zhao, International Journal of Electrochemical Science, 2012, 7, 2164-2174.
7. S. M. Abbas, S. T. Hussain, S. Ali, N. Ahmad, N. Ali, S. Abbas, Journal of Materials Science, 2013, 48, 5429-5436.
8. C. Q. Zhang, J. P. Tu, Y. F. Yuan, X. H. Huang, X. T. Chen, F. Mao, Journal of the Electrochemical Society, 2007, 154, A65-A69.
9. Q. S. Xie, X. Q. Zhang, X. B. Wu, H. Y. Wu, X. Liu, G. H. Yue, Electrochimica Acta, 2014, 125, 659-665.
10. J. P. Liu, Y. Y. Li, X. T. Huang, G. Y. Li, Z. K. Li, Advanced Functional Materials, 2008, 18, 1448-1458.
11. J. P. Liu, Y. Y. Li, R. M. Ding, J. Jiang, Y. Y. Hu, X. X. Ji, Q. B. Chi, Z. H. Zhu, X. T. Huang, Journal of Physical Chemistry C, 2009, 113, 5336-5339.
12. K. T. Park, F. Xia, S. W. Kim, S. B. Kim, T. Song, U. Paik, W. I. Park, Journal of Physical Chemistry C, 2013, 117, 1037-1043.
13. F. Belliard, P. A. Connor, J. T. S. Irvine, Ionics, 1999, 5, 450-454.
14. Y. C. Kong, D. P. Yu, B. Zhang, W. Fang, S. Q. Feng, Applied Physics Letters, 2001, 78, 407-409.
15. L. F. Xu, Y. Guo, Q. Liao, J. P. Zhang, D. S. Xu, Journal of Physical Chemistry B, 2005, 109, 13519-13522.
16. Y. J. Feng, M. Zhang, M. Guo, X. D. Wang, Crystal Growth & Design, 2010, 10, 1500-1507.
17. X. F. Zhou, D. Y. Zhang, Y. Zhu, Y. Q. Shen, X. F. Guo, W. P. Ding, Y. Chen, Journal of Physical Chemistry B, 2006, 110, 25734-25739.
18. J. Y. Choi, R. S. Hsu, Z. W. Chen, Journal of Physical Chemistry C, 2010, 114, 8048-8053.
19. C. C. Chang, H. K. Su, L. J. Her, J. H. Lin, Journal of the Chinese Chemical

RSC Advances Accepted Manuscript

Society, 2012, 59, 1233-1237.

20. X. Yang, Y. L. Xu, H. Zhang, Y. A. Huang, Q. Jiang, C. J. Zhao, Electrochimica Acta, 2013, 114, 259-264.
21. H. Dong, Y. L. Xu, M. D. Ji, H. Zhang, Z. Zhao, C. J. Zhao, Electrochimica Acta, 2015, 151, 118-125.
22. L. J. An, J. Wang, T. F. Zhang, H. L. Yang, Z. H. Sun, Advanced Materials Research, 2012. 380, 335-338.
23. F. Tokiwa, K. Tsujii, Bulletin of the Chemical Society of Japan, 1973, 46, 2684-2686.
24. M. Kruk, M. Jaroniec, Chemistry of Materials, 2001, 13, 3169-3183.
25. A.Vu, Y. Q. Qian, A. Stein, Advanced Energy Materials, 2012, 2, 1056-1085.
26. H. B. Wang, Q. M. Pan, Y. X. Cheng, J. W. Zhao, G. P. Yin, Electrochimica Acta, 2009, 54, 2851-2855.
27. X. H. Huang, X. H. Xia, Y. F. Yuan, F. Zhou, Electrochimica Acta, 2011, 56, 4960-4965.
28. F. Belliard, J. T. S. Irvine, Journal of Power Sources, 2001, 97-98, 219-222.
29. M. S. Wu, H. W. Chang, Journal of Physical Chemistry C, 2013, 117, 2590-2599.
30. Y. Sharma, N. Sharma, G. V. S. Rao, B. V. R. Chowdari, Advanced Functional Materials, 2007, 17, 2855-2861.
31. L. Qiao, X. H. Wang, X. L. Sun, X. W. Li, Y. X. Zheng, D. Y. He, Nanoscale, 2013, 5, 3037-3042.
32. M. Ahmad, Y. Y. Shi, A. Nisar, H. Y. Sun, W. C. Shen, M. Wei, J. Zhu, Journal of Materials Chemistry, 2011, 21, 7723-7729.
33. X. J. Zhu, Y. W. Zhu, S. Murali, M. D. Stoller, R. S. Ruoff, Journal of Power Sources, 2011, 196, 6473-6477.
34. S. L. Shi, Y. G. Liu, J. Y. Zhang, T. H. Wang, Chinese Physics B, 2009, 18, 4564-07.
35. Z. W. Fu, F. Huang, Y. Zhang, Y. Chu, Q. Z. Qin, Journal of the Electrochemical Society, 2003, 150, A714-A720.
36. L. Zhou, D. Y. Zhao, X. W. Lou, Advanced Materials, 2012, 24, 745-748.

RSC Advances Accepted Manuscript

37. Q. Cao, H. P. Zhang, G. J. Wang, Q. Xia, Y. P. Wu, H. Q. Wu, Electrochemistry Communications, 2007, 9, 1228-1232.

38. Z. X. Yang, G. D. Du, Q. Meng, Z. P. Guo, X. B. Yu, Z. X. Chen, T. L. Guo, R. Zeng, Journal of Materials Chemistry, 2012, 22, 5848-5854.

Table 1. BET surface area, Pore volume and Pore size of ZnO/KB composite and KB

Samples	$S_{BET}(m^2g^{-1})$	$V_{total}(cm^3g^{-1})$	$D_{Pore}(Å)$
ZnO/KB	549.54	0.69	36.30
KB	1265.92	3.01	71.99

Table 2. Impedance parameters of the as-obtained samples[a].

Samples	R_e (Ω)	R_{ct} (Ω)	$\sigma_w(\Omega cm^2s^{-1})$
ZnO	11.52	338.74	92.48
ZnO/KB	3.49	116.14	19.53

[a]R_e: electrolyte resistance; R_{ct}: charge transfer resistance; σ_w: Warburg impedance

Figure Captions

Fig. 1. Scheme of ZnO/KB forming mechanism.

Fig. 2. XRD patterns of pure KB, ZnO, ZnO/KB nanocomposite, and JCPDS of normal ZnO.

Fig. 3. TG curves for ZnO/KB composite.

Fig. 4. N_2 adsorption-desorption isotherms of KB(a) and ZnO/KB(b). The insets show the corresponding pore size distributions.

RSC Advances Accepted Manuscript

Fig. 5. (a.b)SEM images of pure ZnO, (c,d) SEM images of KB and ZnO/KB composite

Fig. 6. Low magnification TEM image (a) and HRTEM image (b) of ZnO/KB nanocomposite.

Fig. 7. Elemental mapping for the particles of sample ZnO/KB.

Fig.8.(a)CV curves of the ZnO/KB composite and ZnO at0.1mV/s; (b)Charge–discharge curves of ZnO/KB composite and ZnO at 100 mA/g; (c)Cycling performance of ZnO/KB composite, bare ZnO, ZnO from ZnO/KB and KB at 100 mA/g;(d)Rate capabilities of the three samples at various current densities.

Fig. 9. (a) EIS spectra of ZnO/KB composite in the frequency range between 0.01 Hz and100 kHz; (b) The relationship between Z' and $\omega^{-1/2}$ at low frequency for ZnO and ZnO/KB.

RSC Advances Accepted Manuscript

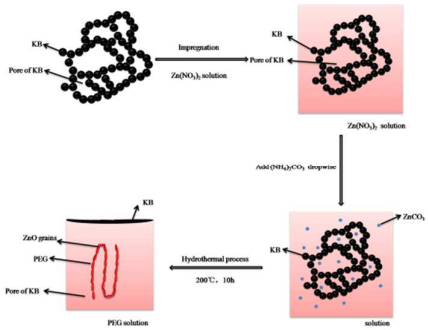

Fig. 1. Scheme of ZnO/KB forming mechanism.

RSC Advances Accepted Manuscript

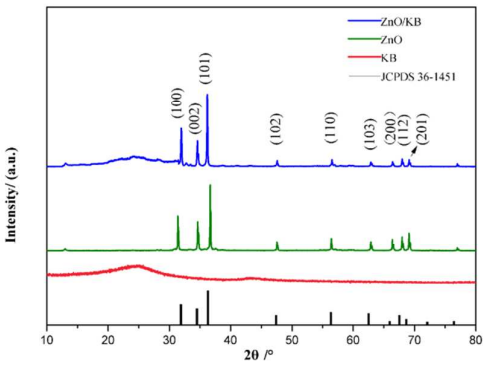

Fig. 2. XRD patterns of pure KB, ZnO, ZnO/KB nanocomposite, and JCPDS of normal ZnO.

RSC Advances Accepted Manuscript

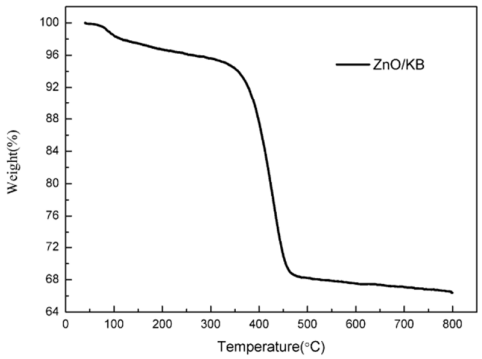

Fig. 3. TG curves for ZnO/KB composite.

RSC Advances Accepted Manuscript

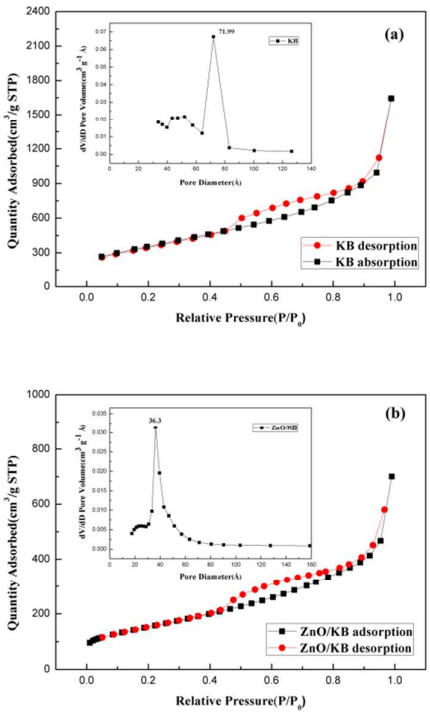

Fig. 4. N_2 adsorption-desorption isotherms of KB(a) and ZnO/KB(b). The insets show the corresponding pore size distributions.

RSC Advances Accepted Manuscript

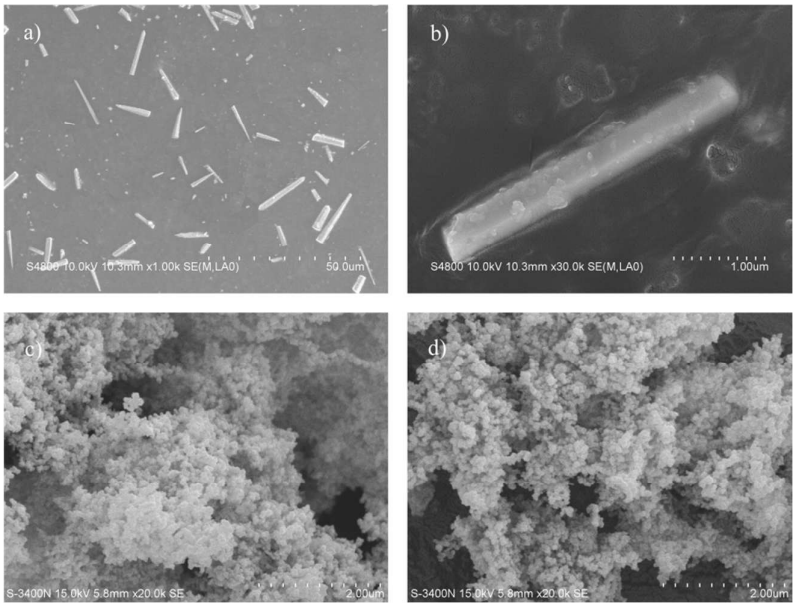

Fig. 5. (a.b)SEM images of pure ZnO, (c,d) SEM images of KB and ZnO/KB composite

RSC Advances Accepted Manuscript

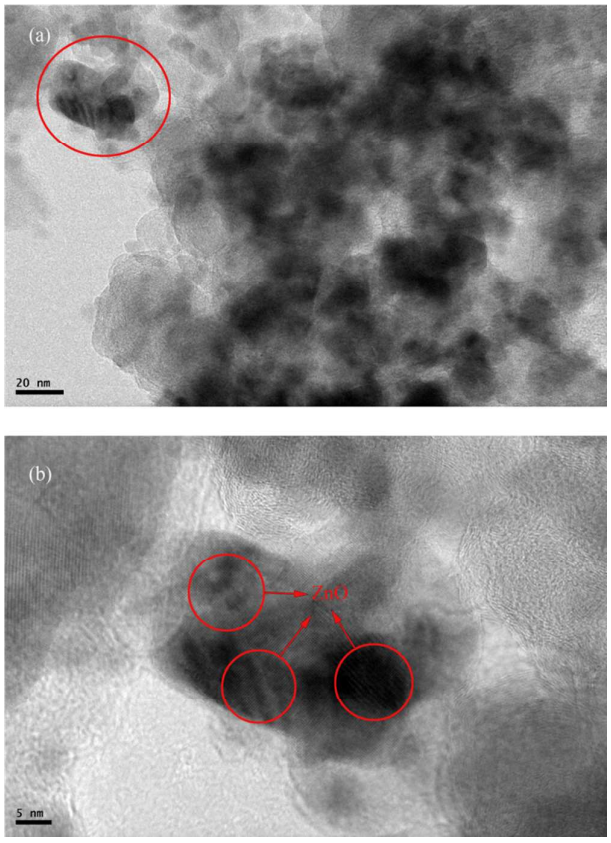

Fig. 6. Low magnification TEM image (a) and HRTEM image (b) of ZnO/KB nanocomposite.

RSC Advances Accepted Manuscript

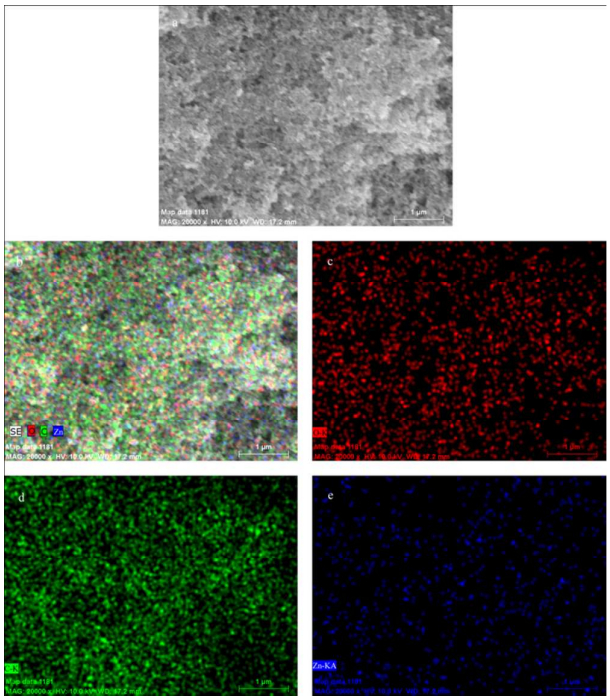

Fig. 7. Elemental mapping for the particle of sample ZnO/KB.

RSC Advances Accepted Manuscript

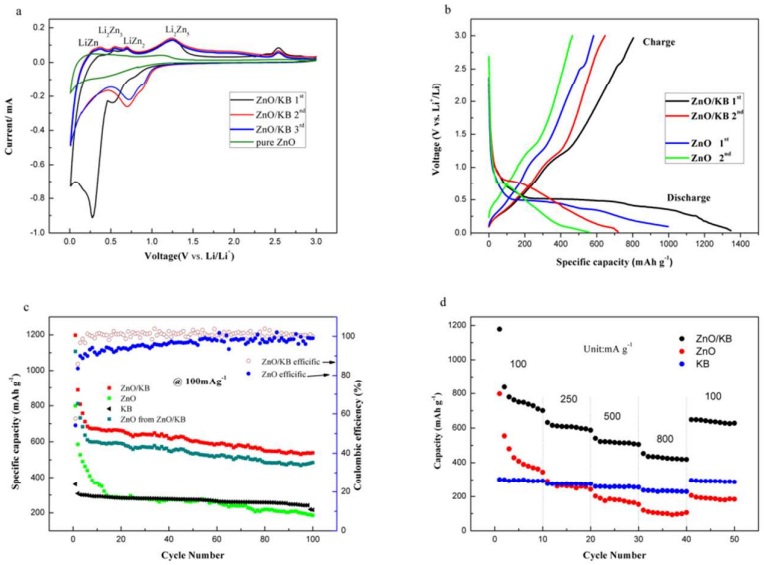

Fig.8.(a)CV curves of the ZnO/KB composite and ZnO at 0.1mV/s; (b)Charge–discharge curves of ZnO/KB composite and ZnO at 100 mA/g; (c)Cycling performance of ZnO/KB composite, bare ZnO, ZnO from ZnO/KB and KB at 100 mA/g;(d)Rate capabilities of the three samples at various current densities.

RSC Advances Accepted Manuscript

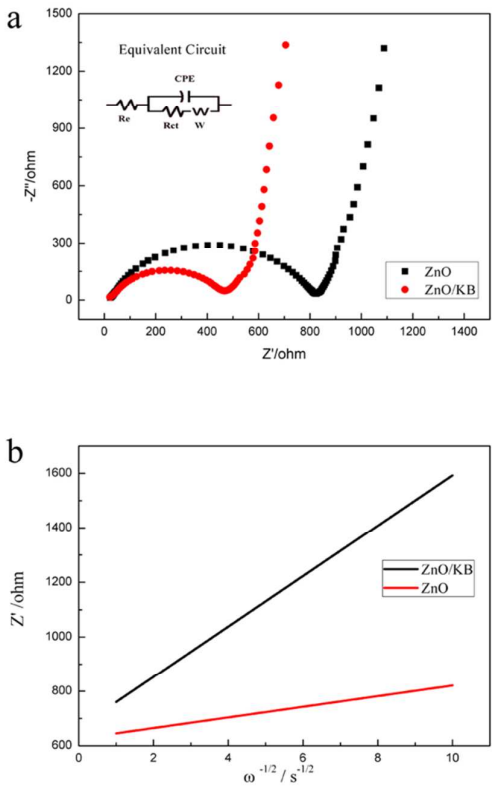

Fig. 9. (a) EIS spectra of ZnO/KB composite in the frequency range between 0.01 Hz and100 kHz; (b) The relationship between Z' and $\omega^{-1/2}$ at low frequency for ZnO and ZnO/KB.

RSC Advances Accepted Manuscript